Progress In Electromagnetics Research C, Vol. 171, 49–58, 2026

(Received 22 April 2026, Accepted 22 May 2026, Scheduled 29 May 2026)

Electromagnetic Scattering Characteristics of Dielectric-Coated Targets Using the Characteristic Mode Basis Function Method

Jiayu Yan[1], Zhonggen Wang[1], Wenyan Nie[2,*], and Han Lin[1]

[1]*School of Electrical and Information Engineering, Anhui University of Science and Technology, Huainan 232001, China*
[2]*School of Mechanical and Electrical Engineering, Huainan Normal University, Huainan 232001, China*

ABSTRACT: Analyzing the electromagnetic scattering of electrically large targets with complex coatings presents significant computational challenges. This study proposes a highly efficient hybrid acceleration method within the Electric Field Integral Equation (EFIE) framework, combining the Thin Dielectric Sheet (TDS) approximation, Characteristic Mode Analysis (CMA), and Adaptive Cross Approximation (ACA). First, a generalized TDS formulation maps dual-layer equivalent currents onto a single-surface model, substantially reducing the number of initial unknowns while preserving physical consistency. Next, domain decomposition and CMA are used to construct a reduced-order matrix, enabling a direct, non-iterative solution that fundamentally bypasses the traditional convergence bottlenecks. Finally, the ACA compresses well-separated far-field interactions to further minimize the computational and memory costs. Comprehensive numerical experiments calculating the radar cross section (RCS) of electrically large coated targets demonstrate that the proposed hybrid scheme offers superior accuracy and drastically reduces matrix storage and computation time compared to conventional full-wave direct solvers and traditional TDS-EFIE (electric and magnetic) formulations.

1. INTRODUCTION

Driven by the continuous advancement of modern detection technologies, the electromagnetic stealth requirements for high-value targets have become increasingly strict. Traditionally, electromagnetic scattering analysis of standard targets relies heavily on full-wave numerical techniques, such as the Method of Moments (MoM) [1, 2]. However, for electrically large targets, the dense matrices of the MoM cause severe memory and computational bottlenecks. To alleviate it, various fast algorithms have been developed to significantly accelerate matrix compression and filling. Examples include the Multilevel Fast Multipole Algorithm (MLFMA) [3], Characteristic Basis Function Method (CBFM) [4], Domain Decomposition Method (DDM) [5], and Adaptive Cross Approximation (ACA) [6]. While these methods are highly effective for perfect conductors, analyzing dielectric-coated targets remains challenging. High-fidelity solutions necessitate the Volume-Surface Integral Equation (VSIE) [7] or PMCHWT [8–10] formulations, which inherently require two-layer or three-dimensional volumetric discretization. The resulting massive unknowns generate highly ill-conditioned matrices, causing severe convergence failures in iterative algorithms, even with ACA or MLFMA acceleration. To fundamentally address this issue, Characteristic Mode Analysis (CMA) [11–13] is introduced as a powerful dimension-reduction technique. CMA partitions the target into subdomains to extract physically significant characteristic modes. These excitation-independent orthogonal basis functions then transform a massive system into a low-dimensional direct-solution problem. Consequently, this method effectively circumvents iterative convergence issues.

To overcome the computational burden imposed by two-layer discretization, traditional Impedance Boundary Conditions (IBCs) [14–16] have been widely adopted, successfully reducing the physical model to an equivalent single-layer problem. However, when dealing with highly curved surfaces or oblique incidence at large grazing angles, the standard IBC inevitably introduces significant errors because it neglects the normal polarization effects and phase delay along the thickness direction within the dielectric layer [17, 18]. To reconcile the computational efficiency of single-layer modeling with physical rigor, the Thin Dielectric Sheet (TDS) [19, 20] approximation, derived from the volume equivalence principle, has emerged as a superior alternative. By incorporating a polarization contrast coefficient and physical thickness offset, the TDS method accurately compensates for the discontinuity of the electric field, thereby perfectly restoring the true polarization and phase information within a single-layer mesh framework. Unlike conventional standard TDS models, which are restricted solely to electric field corrections, a more rigorous generalized TDS model addresses both the electric and magnetic fields simultaneously. By introducing both electric and magnetic polarization contrast coefficients along with a physical thickness offset, this model accurately compensates for the dual discontinuities of electromagnetic fields as they traverse the dielectric layer. Consequently, it perfectly restores the true polarization, magnetization, and phase information within a single-

---

* Corresponding author: Wenyan Nie (wynie5240@163.com).

doi:10.2528/PIERC26042202

Published by THE ELECTROMAGNETIC ACADEMY

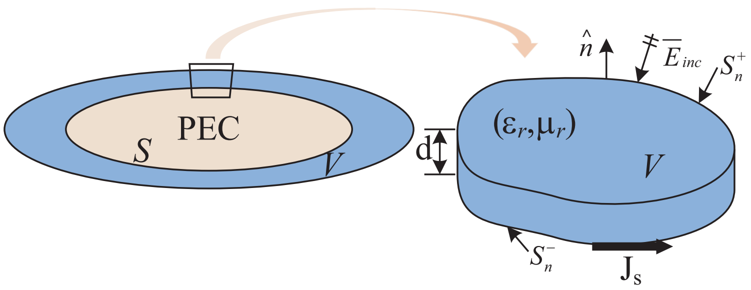

FIGURE 1. Schematic diagram of the equivalent TDS model.

layer mesh framework. The TDS formulation effectively corrects these theoretical deficiencies. However, if the underlying solver continues to rely on conventional MoM, the resulting dense impedance matrix remains ill-equipped for complex, large-scale targets [21, 22].

Driven by these considerations, this study proposes a novel hybrid acceleration scheme based on the TDS-EFIE (Electric Field Integral Equation). This scheme deeply integrates CMA and the ACA algorithm to efficiently and accurately analyze the scattering of complex, electrically large coated targets. First, a rigorous TDS integral model incorporating polarization corrections was established on the coated surface, and characteristic mode basis functions were utilized to drastically reduce the dimensionality of the system. Second, a hybrid strategy is introduced to construct the reduced-order matrix. Rigorous full-precision numerical integration is employed for strongly coupled near-field regions. Meanwhile, the ACA algorithm is directly applied to weakly coupled far-field regions for rapid matrix compression and filling. Numerical examples demonstrate that, while maintaining rigorous physical accuracy, the proposed scheme significantly reduces memory consumption and enhances the overall computational efficiency.

2. THEORY

2.1. Establishment of the TDS-EFIE

First, physical and equivalent models were established (Fig. 1). A perfect electric conductor (PEC) is coated with a lossy dielectric layer of thickness d, permittivity ε_r, and permeability μ_r. S_n^+ and S_n^- denote the top and bottom surfaces of the coating. $\hat{n}$ is the outward normal unit vector of S_n^+. When this coating is much thinner than the wavelength, the TDS approximation reduces the three-dimensional layer to a two-dimensional equivalent surface. By retaining only the normal electric and tangential magnetic field components, this projection significantly reduces the dimensionality of the subsequent modeling.

For a PEC target coated with a lossy dielectric material, under illumination by an external electromagnetic wave, the total tangential electric field on its surface must be zero, according to the boundary conditions on the target surface:

$$\left[\mathbf{E}^{inc}(\mathbf{r})+\mathbf{E}^{sca}(\mathbf{r})\right]_{\text{tan}}=0 \tag{1}$$

In Eq. (1), $\mathbf{r}$ denotes the position vector of the observation point on the target surface, $\mathbf{E}^{inc}(\mathbf{r})$ the incident electric field, $\mathbf{E}^{sca}(\mathbf{r})$ the scattered electric field, and the subscript "tan" indicates the tangential component of the electric field. This scattered electric field is generated jointly by the conductor surface and dielectric coating layer and can be linearly superposed as

$$\mathbf{E}^{sca}(\mathbf{r})=\mathbf{E}^{sca}_{pec}(\mathbf{r})+\mathbf{E}^{sca}_{die}(\mathbf{r}) \tag{2}$$

According to the equivalence principle, the purely conductive part of the scattered electric field, $\mathbf{E}^{sca}_{pec}(\mathbf{r})$, generated by the equivalent induced surface current $\mathbf{J_s}$ on the conductor surface can be expressed as

$$\mathbf{E}^{sca}_{pec}(\mathbf{r})=-j\omega\mu_0\int_S\left(\mathbf{J_s}(\mathbf{r}')+\frac{1}{k_0^2}\nabla\nabla'\cdot\mathbf{J_s}(\mathbf{r}')\right)G(\mathbf{r},\mathbf{r}')dS' \tag{3}$$

where j is the imaginary unit; ω is the angular frequency of the incident wave; $\mathbf{r}$ and $\mathbf{r}'$ denote the position vectors of the observation point and the source point, respectively; ∇ and ∇' represent the del operators with respect to the unprimed and primed coordinates, respectively; $G(\mathbf{r},\mathbf{r}')=\frac{e^{-jk_0|\mathbf{r}-\mathbf{r}'|}}{4\pi|\mathbf{r}-\mathbf{r}'|}$ is the scalar Green's function in free space; $k_0=\omega\sqrt{\mu_0\varepsilon_0}$ is the free-space wavenumber, with μ_0 and ε_0 being the permeability and permittivity of the free space, respectively.

When the physical thickness of the coating layer is much smaller than the operating wavelength, the TDS approximation can be introduced to reduce the dimensionality of the model. This approximation neglects the tangential electric field and normal magnetic field components inside the coating, retaining only the normal electric field and tangential magnetic field components inside the coating. Further incorporating the current continuity condition at the interface, the scattered electric field generated by the dielectric layer $\mathbf{E}^{sca}_{die}(\mathbf{r})$ can be rigorously expressed as

$$\begin{aligned}\mathbf{E}^{sca}_{die}(\mathbf{r})=-j\omega\mu_0\Bigg[&\int_S\hat{n}'d\chi G(r,r')\nabla'\bullet\mathbf{J_s}dS'\\&+\frac{\nabla}{k_0^2}\int_S\chi(G(r,r')-G_d(r,r'))\nabla'\bullet\mathbf{J_s}dS'\\&+(1-\mu_r)\int_S d\nabla G(r,r')\times(\hat{n}'\times\mathbf{J_s})dS'\Bigg]\end{aligned} \tag{4}$$

In Equations (2)–(4), the electric polarization contrast parameter $\chi=1/\epsilon_r-1$ is introduced. Here, ϵ_r and μ_r are the relative permittivity and relative permeability of the coating dielectric, respectively, and $\hat{n}'$ is the outward unit normal vector on the conductor surface. Furthermore, to accurately compensate for the normal phase delay caused by the electromagnetic wave penetrating the coating, a modified Green's function G_d with a physical thickness offset is introduced as:

$$G_d(\mathbf{r}, \mathbf{r}') = \frac{e^{-jk_0|\mathbf{r}-(\mathbf{r}'+d\hat{n}')|}}{4\pi|\mathbf{r}-(\mathbf{r}'+d\hat{n}')|} \tag{5}$$

By combining the scattered field contributions from the conductor and the dielectric and substituting them into the total field boundary condition, the Thin Dielectric Sheet Approximation Electric Field Integral Equation (TDS-EFIE) containing only a single unknown surface current is obtained as follows:

$$\begin{aligned}\mathbf{E}_{\text{tan}}^{inc}(\mathbf{r}) = j\omega\mu_0 \Bigg[& \frac{1-\mu_r}{2}\mathbf{J_s}d + G(r,r')\left(\mathbf{J_s} + \hat{n}'d\chi\nabla' \times \mathbf{J_s}\right)dS' \\ & + \frac{\nabla}{k_0^2}\int_s (G(r,r') + \chi G(r,r') - \chi G_d(r,r'))\nabla' \times \mathbf{J_s}dS' \\ & + (1-\mu_r)\int_s d\nabla G(r,r') \times (\hat{n}' \times \mathbf{J_s})dS' \Bigg]_{\text{tan}}\end{aligned} \tag{6}$$

Applying RWG vector basis functions and Galerkin testing to discretize this integral equation transforms it into a dense complex-coefficient linear system, $\mathbf{ZJ} = \mathbf{V}$. The impedance matrix $\mathbf{Z}$ here rigorously accounts for the normal thickness offset of the coating material, the dielectric polarization discontinuity, and magnetization weighting effect based on the underlying physical mechanism. After constructing this high-precision impedance matrix, its real and imaginary parts can be extracted to formulate a generalized eigenvalue equation. The CMA method is then introduced to extract the target's eigen-physical modes, ultimately enabling the reduction and fast solution of a large impedance matrix.

2.2. Method of Characteristic Mode Basis Functions

For electrically large dielectric-coated targets, the traditional MoM generates an extremely large dense impedance matrix. The direct inversion or iterative solution of such a matrix faces severe bottlenecks in terms of memory consumption and computational complexity. To overcome this computational limitation, this study adopts the Characteristic Mode basis function method based on the domain decomposition strategy for matrix order reduction. The core idea of domain decomposition is "divide and conquer". First, low-order, effective characteristic modes reflecting the target's intrinsic resonance are extracted within each subdomain. Then, a linear combination of these local modes is used to approximate the global induced current. This approach significantly reduces the degrees of freedom of the global system unknowns while maintaining full-wave accuracy.

First, according to the geometric topology and electrical size of the target, the continuous surface mesh is divided into M mutually independent subdomains. To reduce the edge current singularity error caused by artificial physical truncation, the boundaries of each subdomain are usually moderately extended (an overlapping region extended by 0.15λ outward along the boundary). Assuming that the $i_{th}(i = 1, 2, \ldots, M)$ subdomain contains N_i RWG vector basis functions, the originally large and disordered global impedance matrix equation can be reorganized into the following block form:

$$\begin{bmatrix} \mathbf{Z}_{11} & \mathbf{Z}_{12} & \mathbf{Z}_{13} & \cdots & \mathbf{Z}_{1M} \\ \mathbf{Z}_{21} & \mathbf{Z}_{22} & \mathbf{Z}_{23} & \cdots & \mathbf{Z}_{2M} \\ \vdots & \vdots & \vdots & \vdots & \vdots \\ \mathbf{Z}_{M1} & \mathbf{Z}_{M2} & \mathbf{Z}_{M3} & \cdots & \mathbf{Z}_{MM} \end{bmatrix} \begin{bmatrix} \mathbf{J}_1 \\ \mathbf{J}_2 \\ \vdots \\ \mathbf{J}_M \end{bmatrix} = \begin{bmatrix} \mathbf{E}_1 \\ \mathbf{E}_2 \\ \vdots \\ \mathbf{E}_M \end{bmatrix} \tag{7}$$

where $\mathbf{Z}_{ij}$ is the $N_i \times N_j$ dimensional sub-impedance matrix representing the electromagnetic coupling between the i_{th} and j_{th} subdomains, with $i, j \in \{1, 2, \ldots, M\}$ being the subdomain indices. N_i and N_j denote the numbers of RWG basis functions in the i_{th} and j_{th} subdomains, respectively.

After obtaining the block matrix structure, characteristic mode basis functions are independently constructed for each subdomain: first, extract the self-impedance matrix of a single subdomain. The real and imaginary parts of this impedance matrix are $\mathbf{R}$ and $\mathbf{X}$, respectively. Then, $\mathbf{Z} = \mathbf{R} + j\mathbf{X}$. M is chosen as $\mathbf{R}$ and let $\nu_n = 1 + j\lambda_n$, obtaining the generalized eigenvalue problem:

$$\mathbf{XJ}_n = \lambda_n\mathbf{RJ}_n \tag{8}$$

where $\mathbf{R}$ physically represents the radiated power of the modes; $\mathbf{X}$ relates to the stored reactive power; n denotes the index of the characteristic modes within the subdomain; and λ_n is the eigenvalue characterizing the resonant behavior and modal phase of the n_{th} mode.

All eigenvalues and eigenvectors of the subdomains were obtained. Then, physically effective characteristic modes were selected according to the modal significance (MS), and nonphysical spurious modes were discarded. The selected eigenvectors were used as CMs for that subdomain to represent the current distribution within the subdomain.

$$MS = \left|\frac{1}{1 + j\lambda_n^m}\right| \tag{9}$$

where λ_n represents the eigenvalue of the n_{th} mode. To ensure strict numerical stability, a mathematically bounded selection strategy is implemented by exploiting the intrinsic orthogonality of characteristic modes. This orthogonality effectively diagonalizes the reduced sub-matrix, analytically governing its condition number κ by the reciprocal of the minimum Modal Significance ($\kappa = 1/MS$). Therefore, imposing a rigid threshold τ (discarding modes with $MS \leq \tau$) mathematically bounds the condition number to a stable regime ($\kappa \leq 1/\tau$), systematically eliminating degenerate or spurious modes that exhibit $MS \to \infty$ and drive $\kappa \to \infty$. A detailed quantitative analysis regarding the optimal selection of τ and its numerical validation on matrix stability is presented in Section 4.1. By continuously monitoring κ during the decomposition process, this theoretically grounded criterion retains only a small number of physically effective, low-order modes to form the characteristic basis function matrix $\mathbf{J}_i^{CM}$ for the i_{th} subdomain. This basis function is then used to achieve a sparse transformation of the subdomain current:

$$\mathbf{J}_i = \mathbf{J}_i^{CM}\alpha_i \tag{10}$$

where α_i is the expansion coefficient corresponding to the characteristic mode basis functions, and its number is much smaller than the number of unknowns N_i in the original subdomain. Substituting the expansion relations of all subdomains into the original matrix equation yields a reduced system with significantly smaller dimensions. This reduced system can be efficiently solved using direct methods (LU decomposition). Consequently, this approach requires no iterations, fundamentally avoiding the convergence problems associated with iterative solvers.

2.3. ACA-accelerated Computation

When the CMA is used to construct the reduced matrix, the overall impedance matrix is partitioned into several sub-block matrices. The diagonal and near-neighbor blocks correspond to strong coupling between subdomains and must be computed exactly. Conversely, the far-field sub-block matrices exhibit low-rank properties. They can be rapidly compressed and filled using the ACA algorithm, which significantly reduces both memory consumption and computational cost.

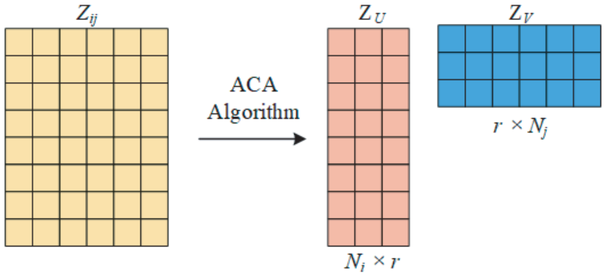

FIGURE 2. Schematic diagram of the far-field impedance matrix decomposition using the ACA algorithm.

As visually illustrated in Fig. 2, the ACA algorithm decomposes the far-field sub-impedance matrix $\mathbf{Z}_{ij}$ (with dimension $N_i \times N_j$ and indices i, j as defined in Section 2.2) into the product of two low-rank factor matrices, $\mathbf{Z}_U$ and $\mathbf{Z}_V$:

$$\mathbf{Z}_{ij}^{N_i\times N_j} \approx \tilde{\mathbf{Z}}_{ij}^{N_i\times N_j} = \mathbf{Z}_U^{N_i\times r}\mathbf{Z}_V^{r\times N_j} \tag{11}$$

where $\mathbf{Z}_U \in C^{N_i\times r}$ and $\mathbf{Z}_V \in C^{r\times N_j}$ represent the generated low-rank compressed matrices, and r is the effective rank of the matrix $\mathbf{Z}_{ij}^{N_i\times N_j}$. For far-field interactions, the rank satisfies $r \leq \min\left(N_i, N_j\right)$. Since only two smaller matrices $\mathbf{Z}_U$ and $\mathbf{Z}_V$ need to be stored, the storage requirement is reduced from the original $N_i \times N_j$ to $r\left(N_i + N_j\right)$.

During the construction of characteristic mode basis functions and the calculation of subdomain mutual coupling, the original full-size submatrices are replaced by the ACA compressed format, and the order of matrix-vector multiplication is optimized:

$$\mathbf{Z}_{ii}^{CM} = -\sum_{j=1, j\neq i}^{M} \mathbf{Z}_U\left(\mathbf{Z}_V\mathbf{J}_j^{CM}\right) \tag{12}$$

where $\mathbf{Z}_{ij}$ and $\mathbf{J}_j^{CM}$ represent the $N_i \times N_j$ matrix and the $N_j \times 1$ vector, respectively. Executing this multiplication operation yields a significantly reduced computational complexity, which decreases from $N_i \times N_j$ to $r(N_i + N_j)$.

By using matrix-vector multiplication operations in the compressed format, the filling time of the reduced matrix can be effectively saved. Expressing the impedance matrix $\mathbf{Z}_{ij}$ in the reduced matrix construction using the compressed format, we obtain

$$\mathbf{J}_i^T\mathbf{Z}_{ij}\mathbf{J}_j = \left[\mathbf{J}_i^T\mathbf{Z}_U\right]\left[\mathbf{Z}_V\mathbf{J}_j\right] \tag{13}$$

This optimization further decreases the computational cost, thereby improving the overall solution efficiency for electrically large dielectric-coated targets while strictly maintaining accuracy.

3. COMPLEXITY ANALYSIS

To quantify the performance advantages of the hybrid method proposed in this section when dealing with electrically large coated targets, a comparative analysis of the computational complexity is conducted between the traditional TDS-EFIE direct-solution method and the CM-ACA hybrid method proposed in this study. Assume that the total number of global unknowns of the target is N, and the target is divided into M subdomains, with the average number of unknowns per subdomain given by $N_i \approx N/M$.

3.1. Complexity of Impedance Matrix Filling

The matrix filling complexity of the traditional method is $O(N^2)$. In the proposed method, although the self-impedance matrices of the diagonal near-field blocks are fully filled, the ACA algorithm is employed for the low-rank compression of the far-field mutual impedance sub-blocks, which account for a large proportion. For a far-field block pair of dimensions $N_i \times N_j$, ACA does not need to compute all matrix elements; instead, by extracting the effective rank, the filling complexity is drastically reduced from the original $O(N_i \times N_j)$ to $O(r(N_i + N_j))$. Because far-field coupling typically exhibits a very strong low-rank property ($r \ll N_i, N_j$), this step reduces the computational cost of the overall matrix filling by orders of magnitude.

3.2. Construction Complexity of Characteristic Mode Basis Functions

The most time-consuming operation in Characteristic Mode Analysis is the generalized eigenvalue decomposition of the self-impedance matrix. For a full matrix, this requires a complexity of $O(N^3)$. By introducing the domain decomposition strategy, the proposed method only requires performing eigenvalue decomposition on M independent sub-impedance matrices, respectively. The complexity for each subdomain is $O((N/M)^3)$, which reduces the overall extraction complexity to $O(N^3/M^2)$. This divide-and-conquer strategy significantly minimizes the computational overhead with rigorous mathematical constraints.

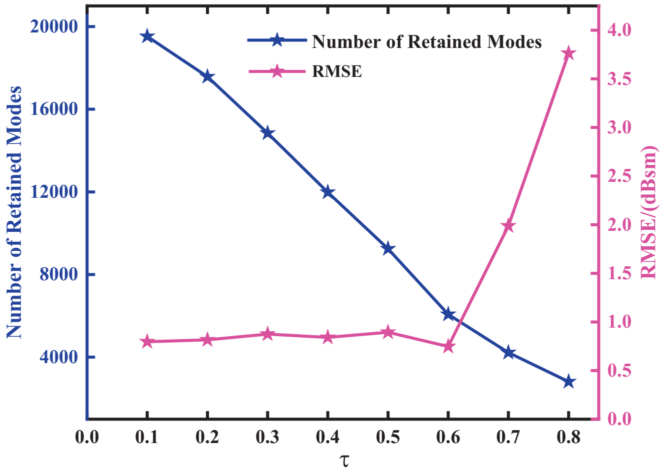

FIGURE 3. Analysis of threshold selection.

3.3. Complexity of Solving the Global Equation

The complexity of solving the global equation using direct LU decomposition in the traditional method is $O(N^3)$. In the proposed method, after efficiently projecting the original MoM impedance matrix onto the extracted characteristic modes, only a small number of effective eigenmodes are retained in each of the subdomains. The degrees of freedom of the global unknowns are thus dramatically reduced from a large number N to the total number of modes K. Consequently, only a very small reduced matrix needs to be solved directly, requiring a complexity of only $O(K^3)$. Because $K \ll N$, the time required for this final direct solution step becomes almost negligible.

In summary, the CM-ACA hybrid scheme proposed in this study achieves rigorous complexity reduction across the entire computational workflow, theoretically confirming its high efficiency in the analysis of electrically large targets.

4. NUMERICAL EXAMPLES AND RESULTS

For reproducibility, reference simulations were performed in Altair FEKO on an Intel-based workstation. The MoM/PMCHWT solver was employed to rigorously handle the penetrable dielectric-conductor boundary. The spherical model used FEKO's standard meshing, while the composite target used a custom mesh with a maximum triangle edge length of 0.035 m. A vertically polarized (VV) plane wave was applied as excitation. Bistatic RCS calculations were accelerated using the Multilevel Fast Multipole Method (MLFMM) with default settings. All configurations were kept strictly consistent with the proposed method to ensure a fair comparison.

4.1. Dielectric-Coated PEC Sphere

The first example analyzes the influence of a dielectric coating material on the radar cross section (RCS) of a PEC sphere. The radius of the conducting sphere was 1 m, the coating thickness d was 0.01 m, the relative permittivity of the dielectric coating material was $\varepsilon_r = 9.0$, the relative permeability was $\mu_r = 1.76 - j4.06$, and the relative surface impedance of the dielectric was $\eta_s = 0.4154 + j0.1258$. The incident wave propagates along the $-Z$ axis at 450 MHz. The conductor surface of the coated target was discretized using triangular elements, resulting in 9876 elements and 14814 unknowns.

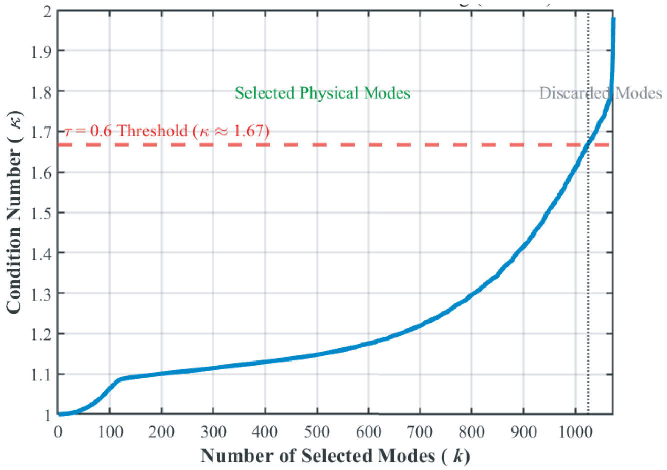

FIGURE 4. Sub-matrix condition number versus the number of selected modes. The red dashed line represents the stability upper bound imposed by $\tau = 0.6$.

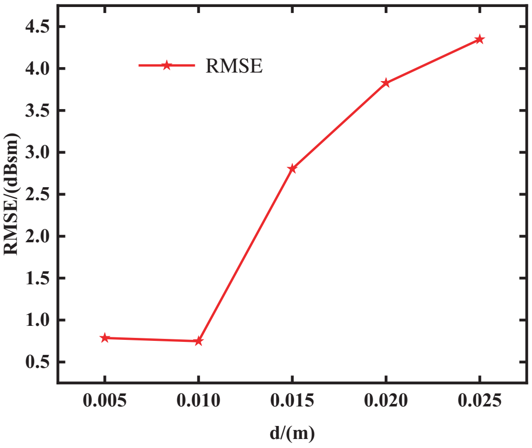

FIGURE 5. Influence of coating thickness on the RMSE.

Before evaluating the far-field scattering, it is essential to determine the optimal threshold τ. Fig. 3 illustrates the trade-off between the number of retained modes and computational accuracy (RMSE) to justify this selection. While increasing τ enhances matrix compression, an excessively high value $(\tau > 0.6)$ discards essential radiating modes, causing a sharp surge in RMSE. Therefore, $\tau = 0.6$ is identified as the optimal inflection point, balancing maximal dimensionality reduction with high-fidelity scattering accuracy.

Having established $\tau = 0.6$ as the optimal physical threshold, it is imperative to verify its mathematical impact on the stability of the reduced system. Fig. 4 plots the continuously monitored sub-matrix condition number κ against the number of selected modes k within a representative subdomain (Block 0) to verify the theoretical bound discussed in Section 2.2. As illustrated, by rigidly applying the $\tau = 0.6$ criterion, the condition number of the selected modes is perfectly capped below

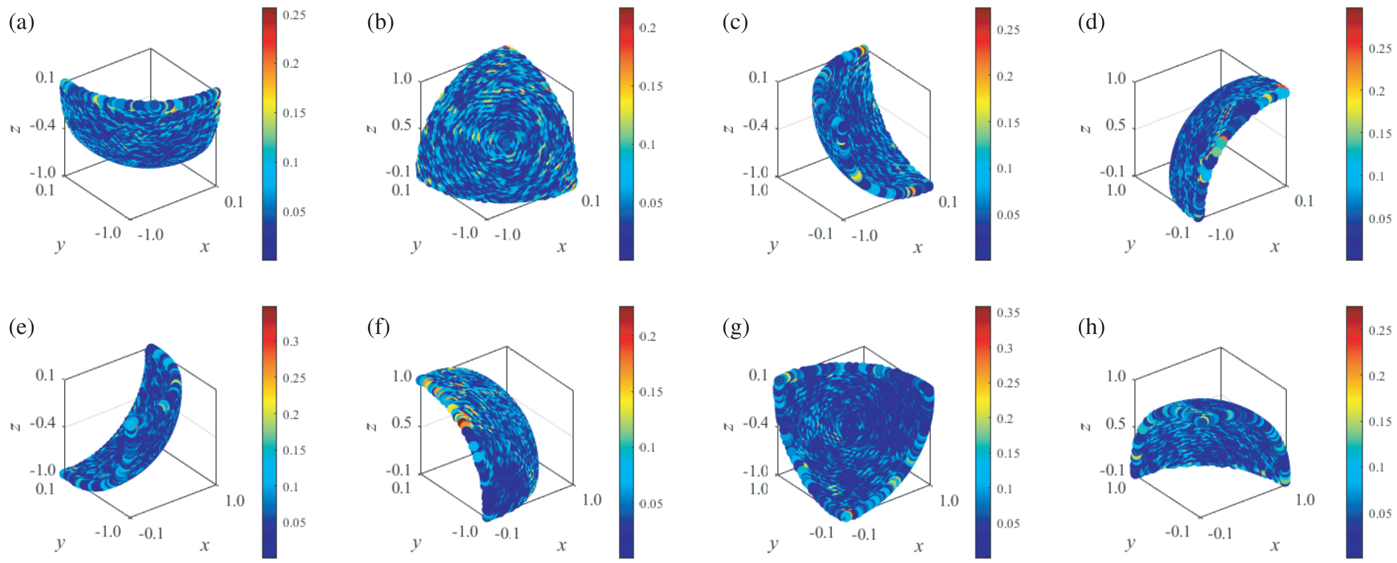

FIGURE 6. Primary characteristic mode current distributions for the eight subdomains of the coated sphere.

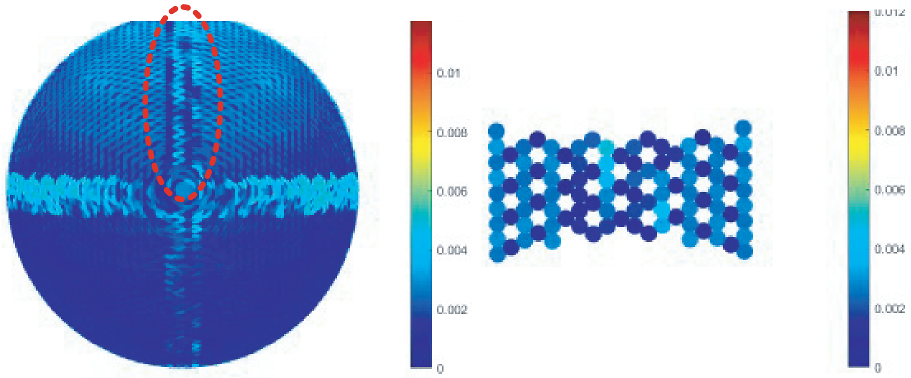

FIGURE 7. Surface current continuity visualization for the domain decomposition strategy.

the theoretical 1.67 safety threshold. Degenerate or spurious modes that would otherwise drive the condition number into exponential divergence are successfully isolated and discarded. This strictly guarantees an iteration-free and robust direct solution for subsequent computations.

As shown in Fig. 5, the characteristic currents are smoothly distributed within each subdomain but exhibit localized concentrations near the truncation boundaries. This distinct current behavior necessitates an overlapping zone to smoothly bridge the characteristic modes across adjacent blocks, ensuring strict physical continuity.

To evaluate the applicable thickness range of the TDS approximation, Fig. 5 illustrates the RMSE versus coating thickness. The error remains exceptionally low for thin coatings ($d \leq 0.010\,\text{m}$). However, as thickness increases, pronounced volume polarization and phase delay degrade the single-layer equivalence, causing a steady rise in RMSE. Consequently, a thickness of 0.01 m is adopted for all subsequent simulations to ensure physical fidelity.

As illustrated in Fig. 6, the extracted dominant modes predominantly feature strongly dipole-like or loop-like resonant current distributions. Physically, the incorporation of a lossy dielectric coating exerts a pronounced damping effect on these natural resonances. Such damping degrades the quality factor of the dominant modes, which effectively suppresses surface currents and attenuates far-field radiation.

Within the domain decomposition framework, Fig. 7 visualizes the smooth transition of surface current J across subdomain boundaries. The rationality of this approach is anchored in the generalized TDS-EFIE formulation, which equivalently incorporates magnetization effects into the impedance matrix via a modified Green's function, leaving J as the sole unknown. Consequently, the demonstrated physical continuity of J rigorously validates the domain decomposition strategy and the overlapping zone configuration. Further quantitative analysis regarding the optimal extension size of this region is detailed in Fig. 8.

Figure 8 illustrates the effect of subdomain extension sizes (0.1λ to 0.3λ) on the solution time and Root Mean Square Error (RMSE). While the solution time increases monotonically with the expansion size, the RMSE drops to a local minimum at 0.15λ. To balance the computational efficiency and approx-

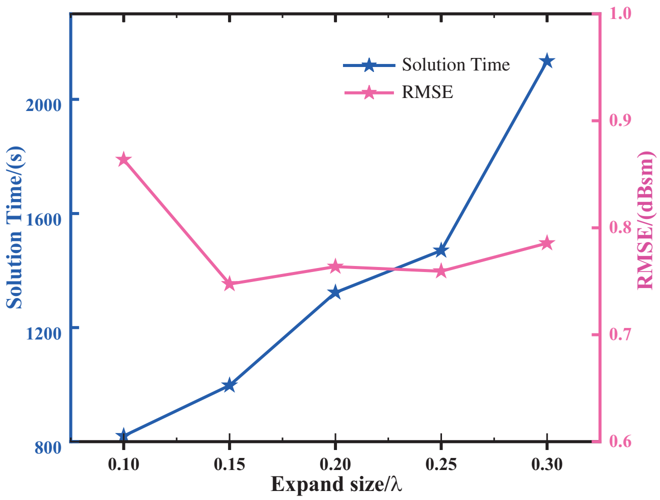

FIGURE 8. Influence of expansion size on solution time and RMSE.

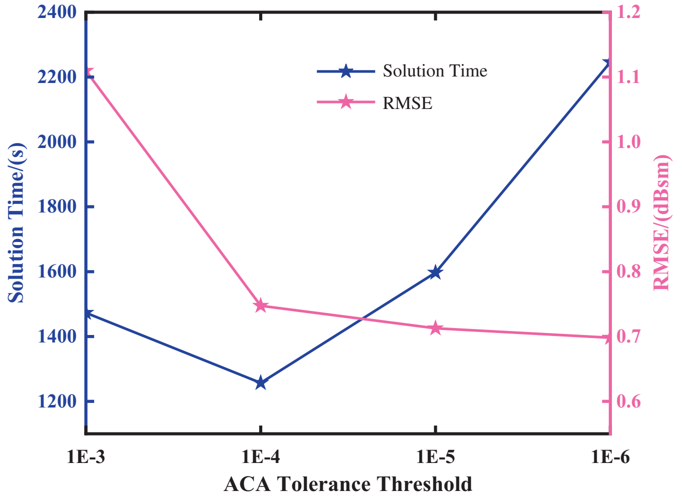

FIGURE 9. Sensitivity analysis of the ACA tolerance threshold in terms of solution time and RMSE.

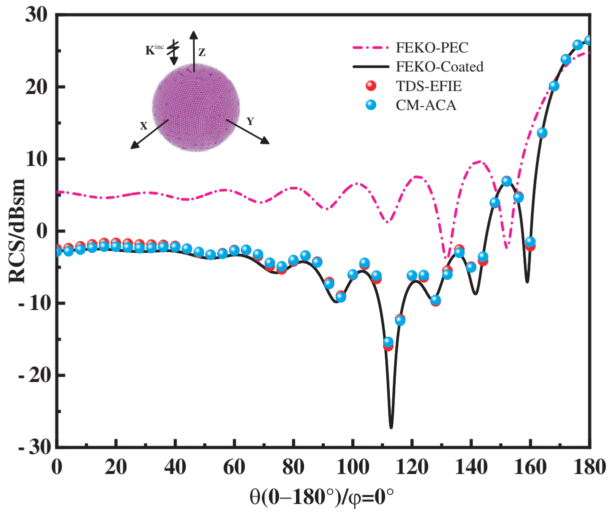

FIGURE 10. Bistatic RCS of a sphere in vertical polarization.

imation accuracy, a 0.15λ overlap was selected as the optimal compromise for this model, which increased the total number of unknowns to 19527.

Figure 9 illustrates the impact of the ACA tolerance threshold on computational performance. As the threshold tightens, the RMSE drops significantly and begins to converge, hitting an 'error floor' bounded by inherent MoM/TDS approximations around the 1E-4 to 1E-5 range. Meanwhile, the solution time exhibits a non-monotonic trend, achieving its minimum at 1E-4 before steadily increasing at tighter tolerances. Therefore, rather than adopting a rigid single value, the optimal threshold can be flexibly adjusted between 1E-4 and 1E-5 in practical computations, allowing for a dynamic balance between computational cost and specific accuracy requirements.

Figure 10 compares the bistatic RCS of this target computed using the traditional TDS-EFIE method (which accounts for both the electric and magnetic properties of the coating), full-wave commercial solver (FEKO-Coated), and the proposed CM-ACA method. In addition, the computed results for a bare PEC sphere (FEKO-PEC) are included as a reference baseline to demonstrate the electromagnetic scattering reduction effect of the proposed dielectric coating.

From a physical perspective in the context of stealth applications, the significant RCS reduction observed in Fig. 10 is a synergistic result of multiple underlying attenuation mechanisms rather than a single effect. First, the introduction of the dielectric coating provides improved impedance matching at the air-target interface, which smoothly transitions the incident wave and minimizes direct specular reflection. Second, the electromagnetic energy that penetrates the coating undergoes strong volume absorption. Given the specific electromagnetic parameters of the coating — particularly the large negative imaginary part of the complex permeability ($\mu_r = 1.76 - j4.06$) — the material exhibits substantial magnetic losses. Consequently, the penetrated electromagnetic wave energy is efficiently dissipated and converted into heat. Therefore, the overall bistatic RCS reduction is driven by a combination of reduced surface reflection and enhanced internal absorption.

The numerical results indicate that the proposed method preserves good accuracy and sharply reduces the matrix filling time at the cost of basis function construction. Compared with the conventional method, the total computation time is reduced by approximately 35.17%, which remarkably enhances the efficiency of solving the electromagnetic scattering of the coated composite target. Furthermore, compared with the bare PEC baseline, the results confirm that the dielectric coating effectively reduces the target's bistatic RCS, particularly exhibiting significant reduction and deep nulls in the broad angular range of 0° to 140°.

4.2. Dielectric-Coated PEC Composite Target

The second example computes the bistatic RCS of a dielectric-coated PEC composite target. The geometry of the target is illustrated in Fig. 13. The target is a capsule-like structure consisting of a central cylinder with a radius of 0.6 m and a height of 1.5 m, capped by two hemispheres at the top and

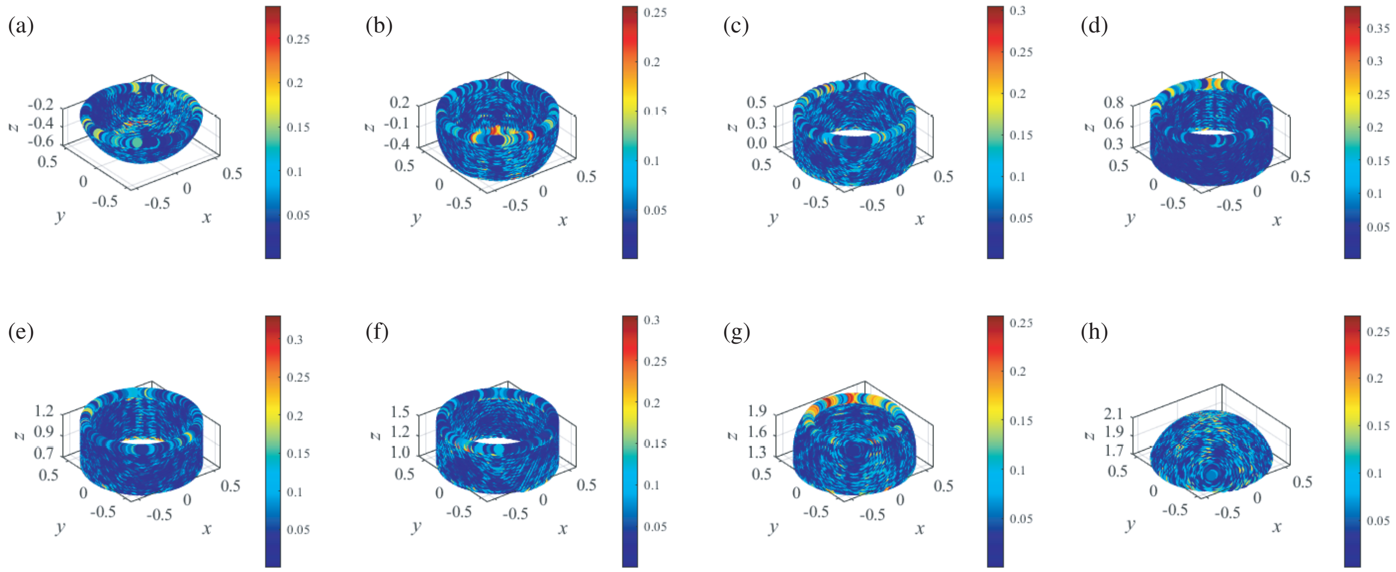

FIGURE 11. Current distributions of the primary characteristic mode for the eight subdomains of the dielectric-coated composite target.

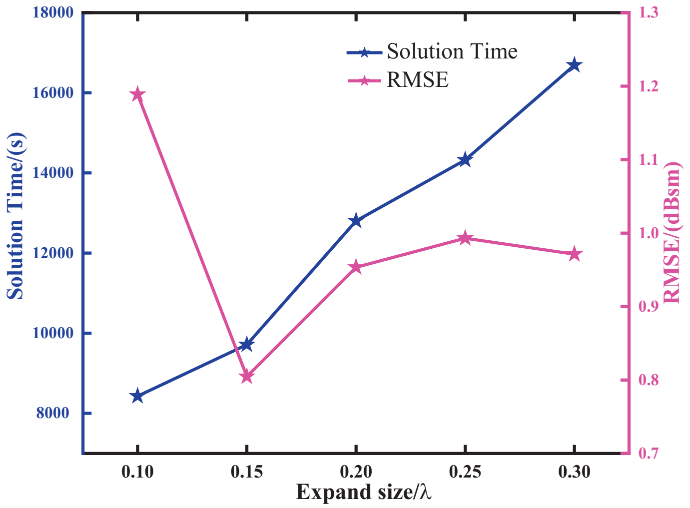

FIGURE 12. Influence of expansion size on solution time and RMSE.

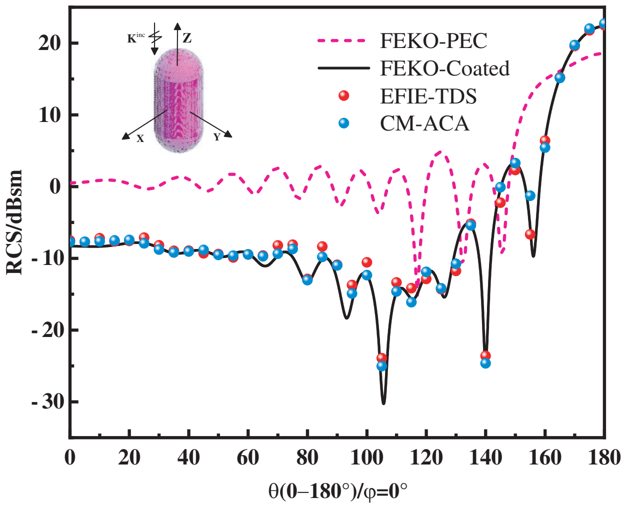

FIGURE 13. Bistatic RCS of the dielectric-coated composite target in vertical polarization.

bottom, each with a radius of 0.6 m. The relative permittivity of the dielectric coating material is $\varepsilon_r = 9.0$; the relative permeability is $\mu_r = 1.76 - j4.06$; the coating thickness is 0.01 m; and the relative surface impedance of the dielectric is $\eta_s = 0.47 + j0.13$. The incident wave at 500 MHz propagates along the $-Z$ axis. The conducting surface of the composite target was discretized into 19702 triangular elements, yielding 29553 initial unknowns.

To implement the Characteristic Mode Analysis, the target was partitioned into eight subdomains along the $-Z$ axis. Fig. 11 shows the current distributions of the dominant characteristic modes extracted for these eight subdomains.

Similar to the spherical case, the current distributions shown in Fig. 11 indicate that the extracted dominant modes primarily exhibit strong dipole-like or loop-like resonances along the complex coated surface. Physically, the lossy dielectric coating introduces a significant damping effect on these natural resonances, lowering their Q-factor to effectively suppress the surface currents and weaken the far-field scattering.

To determine the optimal overlapping zone, Fig. 12 shows extension sizes from 0.1λ to 0.3λ. As the expansion size increased, the solution time exhibited a monotonically increasing trend. In contrast, the RMSE starts at a high peak at 0.1λ, drops sharply to a global minimum at 0.15λ, and then gradually increases. This indicates that an extension of 0.1λ is insufficient to ensure numerical continuity, which leads to significant errors. Therefore, 0.15λ was selected as the optimal compromise, as it achieved the highest accuracy while maintaining a relatively moderate computational time. With this overlap, the total number of unknowns increased to 42709.

Figure 13 compares the VV-polarized bistatic RCS of the target computed using the traditional TDS-EFIE method (which accounts for both the electric and magnetic properties of the coating), full-wave commercial solver (FEKO-Coated), and the

TABLE 1. Influence of expansion size on solution time and RMSE.

Model	Method	Basis function construction(s)	Impedance matrix filling(s)	Solving(s)	Total time(s)
Coated	TDS-EFIE		1441	97	1538
conducting sphere	CM-ACA	478	432	87	997

TABLE 2. Comparison of the proposed method with traditional methods.

Model	Method	Basis function construction(s)	Impedance matrix filling(s)	Solving(s)	Total time(s)
Coated	TDS-EFIE		17197	542	17739
composite target	CM-ACA	1968	7017	730	9715

proposed CM-ACA method. In addition, the computed results for a bare PEC target (FEKO-PEC) are included as a reference baseline to demonstrate the reduction in electromagnetic scattering by the dielectric coating.

As observed in Fig. 13, the proposed CM-ACA method accurately captures the scattering characteristics of the coated composite target. Physically, the significant RCS reduction compared to the bare PEC baseline is achieved through the synergy of impedance matching and volume absorption. For this complex geometry, the lossy coating minimizes the impedance mismatch at multiple interfaces, effectively suppressing specular reflections. Simultaneously, the penetrated wave is efficiently dissipated via magnetic and dielectric losses, driven by the high imaginary part of the permeability ($\mu_r = 1.76 - j4.06$). This confirms that the hybrid solver rigorously models the underlying attenuation mechanisms for complex topologies.

The numerical results indicate that the proposed method preserves good accuracy and sharply reduces the matrix filling time at the cost of basis function construction. Specifically, as observed from the bistatic RCS curves in Fig. 13, the proposed CM-ACA method demonstrates superior precision in capturing the scattering fluctuations compared with the TDS-EFIE method, which exhibits noticeable deviations from the FEKO reference data at certain observation angles. Compared with the conventional method, the total computation time is reduced by approximately 45.23%, which remarkably enhances the efficiency of solving the electromagnetic scattering of the coated composite target. Furthermore, a comparison with the bare PEC baseline physically validated that the dielectric coating effectively reduced the target's bistatic RCS over a wide angular range.

The computation times for the two examples are listed in Tables 1 and 2, respectively. As observed, although the traditional TDS-EFIE method achieves a relatively high accuracy in calculating the RCS of coated targets, it incurs a substantial computational cost. In contrast, the proposed CM-ACA hybrid method significantly reduces the computation time while maintaining high numerical accuracy, thereby drastically improving the overall computational efficiency. Furthermore, the results obtained by the proposed method are in excellent agreement with those calculated using the PMCHW full-wave solver in the commercial software package FEKO, effectively validating its reliability.

5. CONCLUSION

This study investigates the electromagnetic scattering of coated targets. To address the limitation that traditional TDS-EFIE methods are typically restricted to pure dielectric (non-magnetic) coatings, this study adopts an improved TDS-EFIE modeling approach that simultaneously accounts for both the electric and magnetic properties. However, when applied to electrically large targets with a massive number of unknowns, directly solving this generalized equation still suffers from severe computational overhead and long matrix solution times. To overcome this bottleneck, a CM-ACA hybrid acceleration scheme is proposed based on the improved formulation. Compared with the direct solution, the proposed method significantly reduces the computation time without compromising numerical accuracy, thereby drastically improving the overall efficiency. Using this efficient algorithm, the significant RCS reduction performance of the electromagnetic coatings was demonstrated. Furthermore, the results obtained using the proposed method are in excellent agreement with those obtained using the PMCHW full-wave solver in the commercial software FEKO, fully validating its reliability and robustness in analyzing complex coated structures.

ACKNOWLEDGEMENT

This work was supported in part by the Natural Science Research Project of Anhui Educational Committee under Grant No. 2025AHGXZK31006, in part by the Research Foundation of Jiangsu Engineering Research Center for Bionics Control Technology and Equipment under No. FSKZ202503, in part by the Anhui International Joint Research Center for Ancient Architecture Intellisencing and Multi-Dimensional Modeling under No. GJZZX2025KF03, in part by the Graduate Innovation Fund of Anhui University of Science and Technology under grant No. 2026cx2060.

REFERENCES

[1] Harrington, R. F., *Field Computation by Moment Methods*, Macmillan, New York, 1968.

[2] Rao, S., D. Wilton, and A. Glisson, "Electromagnetic scattering by surfaces of arbitrary shape," *IEEE Transactions on Antennas and Propagation*, Vol. 30, No. 3, 409–418, May 1982.

[3] Song, J., C.-C. Lu, and W. C. Chew, "Multilevel fast multipole algorithm for electromagnetic scattering by large complex objects," *IEEE Transactions on Antennas and Propagation*, Vol. 45, No. 10, 1488–1493, Oct. 1997.

[4] Lucente, E., A. Monorchio, and R. Mittra, "An iteration-free MoM approach based on excitation independent characteristic basis functions for solving large multiscale electromagnetic scattering problems," *IEEE Transactions on Antennas and Propagation*, Vol. 56, No. 4, 999–1007, Apr. 2008.

[5] Peng, Z., X.-C. Wang, and J.-F. Lee, "Integral equation based domain decomposition method for solving electromagnetic wave scattering from non-penetrable objects," *IEEE Transactions on Antennas and Propagation*, Vol. 59, No. 9, 3328–3338, Sep. 2011.

[6] Wang, Z., D. Dong, F. Guo, Y. Sun, W. Nie, and P. Wang, "Fast construction of measurement matrix and sensing matrix with dual adaptive cross approximation," *IEEE Antennas and Wireless Propagation Letters*, Vol. 24, No. 1, 13–17, Jan. 2025.

[7] Lu, C. C. and W. C. Chew, "A coupled surface-volume integral equation approach for the calculation of electromagnetic scattering from composite metallic and material targets," *IEEE Transactions on Antennas and Propagation*, Vol. 48, No. 12, 1866–1868, Dec. 2000.

[8] Glisson, A., "An integral equation for electromagnetic scattering from homogeneous dielectric bodies," *IEEE Transactions on Antennas and Propagation*, Vol. 32, No. 2, 173–175, Feb. 1984.

[9] Medgyesi-Mitschang, L. N., J. M. Putnam, and M. B. Gedera, "Generalized method of moments for three-dimensional penetrable scatterers," *Journal of the Optical Society of America A*, Vol. 11, No. 4, 1383–1398, 1994.

[10] Tanaka, T., K. Niino, and N. Nishimura, "Characteristic basis function method combined with Krylov-Calderón preconditioner for PMCHWT formulation," *IEEE Transactions on Antennas and Propagation*, Vol. 72, No. 3, 2578–2591, Mar. 2024.

[11] Harrington, R. and J. Mautz, "Theory of characteristic modes for conducting bodies," *IEEE Transactions on Antennas and Propagation*, Vol. 19, No. 5, 622–628, Sep. 1971.

[12] Capek, M., J. Lundgren, M. Gustafsson, K. Schab, and L. Jelinek, "Characteristic mode decomposition using the scattering dyadic in arbitrary full-wave solvers," *IEEE Transactions on Antennas and Propagation*, Vol. 71, No. 1, 830–839, Jan. 2023.

[13] Wang, Z., P. Wang, Y. Sun, and W. Nie, "Fast analysis of bistatic scattering problems for three-dimensional objects using compressive sensing and characteristic modes," *IEEE Antennas and Wireless Propagation Letters*, Vol. 21, No. 9, 1817–1821, Sep. 2022.

[14] Senior, T. B. A., "Impedance boundary conditions for imperfectly conducting surfaces," *Applied Scientific Research, Section B*, Vol. 8, No. 1, 418–436, 1960.

[15] Glisson, A. W., "Electromagnetic scattering by arbitrarily shaped surfaces with impedance boundary conditions," *Radio Science*, Vol. 27, No. 6, 935–943, 1992.

[16] Senior, T. B. A. and J. L. Volakis, *Approximate Boundary Conditions in Electromagnetics*, IEE Press, London, U.K., 1995.

[17] Volakis, J. L. and T. B. A. Senior, "Application of a class of generalized boundary conditions to scattering by a metal-backed dielectric half-plane," *Proceedings of the IEEE*, Vol. 77, No. 5, 796–805, 1989.

[18] Hoppe, D. J. and Y. Rahmat-Samii, *Impedance Boundary Conditions in Electromagnetics*, CRC Press, Boca Raton, FL, USA, 1995.

[19] Harrington, R. and J. Mautz, "An impedance sheet approximation for thin dielectric shells," *IEEE Transactions on Antennas and Propagation*, Vol. 23, No. 4, 531–534, Jul. 1975.

[20] Newman, E. and M. Schrote, "An open surface integral formulation for electromagnetic scattering by material plates," *IEEE Transactions on Antennas and Propagation*, Vol. 32, No. 7, 672–678, Jul. 1984.

[21] Chew, W. C., H. Y. Chao, T. J. Cui, C. C. Lu, S. Ohnuki, Y. C. Pan, J. M. Song, S. Velamparambil, and J. S. Zhao, "Fast integral equation solvers in computational electromagnetics of complex structures," *Engineering Analysis with Boundary Elements*, Vol. 27, No. 8, 803–823, 2003.

[22] Zhao, K., M. N. Vouvakis, and J.-F. Lee, "The adaptive cross approximation algorithm for accelerated method of moments computations of EMC problems," *IEEE Transactions on Electromagnetic Compatibility*, Vol. 47, No. 4, 763–773, 2005.